Journal of Materials Chemistry B

ROYAL SOCIETY OF CHEMISTRY

PAPER

View Article Online
View Journal | View Issue

Cite this: J. Mater. Chem. B, 2023, 11, 4523

A tunable fluorescent probe for superoxide anion detection during inflammation caused by *Treponema pallidum*†

Weiqiang Lin,‡[a] Jialin Huang,‡[a] Shuang Guo,‡[a] Meijiao Zhao,[a] Xu Chen,[c] Qiuping Shang,[a] Ruoyuan Zhang,[a] Guangfu Liao, *[b] Judun Zheng*[a] and Yuhui Liao *[ad]

Received 5th April 2023,
Accepted 24th April 2023

DOI: 10.1039/d3tb00747b

rsc.li/materials-b

Syphilis, caused by *Treponema pallidum* (*T. pallidum*), is associated with the oxidative stress due to its inflammation-like symptom, and detecting the reactive oxygen species (ROS) is crucial for monitoring the infectious process. Herein, we design and synthesize a perylene-based tunable fluorescent probe, **Per*qdOH***, which can detect endogenous $O_2^{\bullet-}$ during *T. pallidum* infection. The fluorescence peak shifted from 540 nm to 750 nm with increasing $O_2^{\bullet-}$ levels. Besides, both decreased green fluorescence and enhanced red fluorescence could be observed simultaneously during the *in vitro* infection, providing the real-time monitoring of intracellular $O_2^{\bullet-}$ caused by *T. pallidum*. Furthermore, the probe exhibited a remarkable signal in the treponemal lesions on the back of a rabbit model. Taken together, our synthesized **Per*qdOH*** holds great potential for application in clarifying the infectious process caused by *T. pallidum* in real time.

1. Introduction

Syphilis, caused by *Treponema pallidum* subspecies *pallidum* (*T. pallidum*), remains a significant global threat worldwide owing to its potential to cause multiple organ damage and increase the risk of other diseases.[1–3] Similar to inflammation, the accumulation of inflammatory cells such as lymphocytes, neutrophils and macrophages could be found in the lesion site throughout the course of syphilis,[4,5] particularly in the painless chancre of the primary stage and the obvious papule of the secondary stage.[6,7] Indeed, *T. pallidum* infection initially destructs the tissue and triggers an inflammatory response,[8–10] which subsequently activate the production of reactive oxygen species (ROS) to promote the phagocytosis and clearance by macrophages.[8,11–16] The overload ROS plays a central role in the inflammatory disease due to its contribution to trigger oxidative stress and induce inflammation,[17–19] and superoxide radical ($O_2^{\bullet-}$), a primary ROS,[20] has been usually used as a biomarker of inflammation diagnosis.[21,22] The dysregulated $O_2^{\bullet-}$ can lead to oxidative stress,[23] causing harm to biomolecules like DNA, proteins and lipids and inducing apoptosis.[6,24,25] Moreover, the relationship between upregulated ROS and the developed syphilis has been studied,[26,27] suggesting $O_2^{\bullet-}$ may link to the syphilis-related inflammation. Thus, monitoring the level of $O_2^{\bullet-}$ in the living cells and tissues is crucial to determine the extent of oxidative stress, estimate the biological inflammation process,[28,29] and further used for alleviating the inflammation.

To date, fluorescent probes have made significant progress in monitoring oxidative stress.[30–33] Specifically, several reversible fluorescent sensors based on organic molecules have been reported to dynamically monitor the redox couples, including $O_2^{\bullet-}$ and GSH,[34–36] which greatly expanded the detection toolkit for the oxidation state. However, a probe for monitoring syphilis-caused oxidative stress is still lacking. Herein, we develop a perylene-based fluorescent probe (**Per*qdOH***) to detect endogenous $O_2^{\bullet-}$ and determine the inflammatory progress caused by *T. pallidum*. In our design, pyrocatechol was oxidized to carbonyl in the presence of $O_2^{\bullet-}$, causing a red-shift in the fluorescence of our synthesized probe, which could clearly monitor intracellular $O_2^{\bullet-}$ and help ascertain the $O_2^{\bullet-}$ level during treponemal infection *in vitro*. Furthermore, the probe

[a] Molecular Diagnosis and Treatment Center for Infectious Diseases, Dermatology Hospital, Southern Medical University, Guangzhou, 510091, P. R. China. E-mail: liaoyh8@mail.sysu.edu.cn, zhengjd53815@163.com
[b] College of Material Engineering, Fujian Agriculture and Forestry University, Fuzhou, 350002, P. R. China. E-mail: liaogf@mail2.sysu.edu.cn
[c] Department of Infectious Disease, the Fifth Affiliated Hospital, Sun Yat-sen University, Zhuhai, 519000, P. R. China
[d] NHC Key Laboratory of Metabolic Cardiovascular Diseases Research, Ningxia Key Laboratory of Vascular Injury and Repair Research, Ningxia Medical University, Yinchuan, 750004, P. R. China

† Electronic supplementary information (ESI) available. See DOI: https://doi.org/10.1039/d3tb00747b

‡ These authors contributed equally.

can monitor the inflammatory process of the treponemal lesions *in vivo* in real time, which makes it potentially useful to monitor oxidative stress during inflammation caused by *T. pallidum*.

2. Experimental section

2.1 Materials

Dopamine, phorbol-12-myristate-13-acetate (PMA), sodium peroxide, and glutathione (GSH) were purchased from Aladdin (China). Cell counting kit-8 (CCK8) was obtained from Dojindo (Japan). MitoTracker red and Hoechst 33342 were obtained from Invitrogen (USA). Acetic acid, DCM, DMF and MeOH were purchased from Guangzhou chemical Reagent Factory (China). Ultrapure water used in this study was obtained from the Milli-Q water purification system from Millipore.

2.2 Synthesis and characterization of the probe

The reactant (0.394 g, 1.0 mmol) and dopamine (0.306 g, 2.0 mmol) were dissolved in 25 mL acetic acid mixed with NMP, and the mixture was heated at 80 °C for 15 h under a nitrogen atmosphere. After the reaction was completed, the solvent was removed to give the crude product. Then, the crude product was dried and subjected to purification by flash chromatography (DCM: MeOH; 20 : 1) to give probe **Per*qdOH*** as a red solid (0.413 g, 65.3%). Then, ^{1}HNMR, and HR-MS were utilized to characterize the structure of **Per*qdOH***; UV-vis spectrophotometer and fluorescence spectrophotometer were separately used to determine the optical properties.

2.3 Detection of $O_2^{\bullet-}$

Probe **Per*qdOH*** was prepared in DMF, and $O_2^{\bullet-}$ was derived from potassium peroxide. The concentration of **Per*qdOH*** added as a substrate in the detection was 10 μM, and the concentration of $O_2^{\bullet-}$ was 100 μM, while the concentration of GSH used to reduce $O_2^{\bullet-}$ was 500 μM. The spectrum detection was performed 1 min after adding $O_2^{\bullet-}$ or GSH to the substrate using a fluorescence spectrophotometer, and absorption was measured using a UV-vis spectrophotometer similarly.

2.4 Intracellular fluorescence imaging

The exogenous $O_2^{\bullet-}$ was first applied to investigate the imaging capability of **Per*qdOH***. The cell lines used in the experiment were purchased from American Type Culture Collection (ATCC, Manassas, Virginia, USA). B16 cells or RAW 264.7 cells were cultured in 6-well plates at a concentration of 2×10^5 cells per well overnight, and then **Per*qdOH*** was co-cultured with the cells for 4 hours, followed by the addition of $O_2^{\bullet-}$ for another 24 hours. A laser confocal microscope (Nikon A1, Japan) was used for imaging after the cells were stained with Hoechst 33342 for 0.5 h.

As reported, PMA was commonly used to stimulate the generation of endogenous $O_2^{\bullet-}$.[37] The cells were first seeded at a density of 2×10^5 cells mL^{-1} and **Per*qdOH*** was pre-cultured with the cells for 4 h, and 0.5 μg mL^{-1} of PMA was stained at various time points (0 h to 36 h) to investigate the time-dependent manner; for dose-dependent manner, various concentrations (0–1.5 μg mL^{-1}) of PMA were added into the seeded cells for 24 hours. The plates were washed three times with PBS and a laser confocal microscope was used to trace intracellular fluorescence.

2.5 Fluorescence detection after *T. pallidum* infection *in vitro* and *in vivo*

For *in vitro* detection, RAW 264.7 cells (2×10^5 cells mL^{-1}, 2 mL) were first seeded in the plates, and different MOIs (from 1 : 10 to 1 : 1000) of *T. pallidum* were co-cultured with RAW 264.7 cells followed by the pre-incubated **Per*qdOH***. The fluorescence image was then taken using a laser confocal microscope.

The experimental procedures were approved by the Institute of Pharmacology and Toxicology Academy of Military Medical Sciences PLA, Peop. Rep. China Ethical Committee on Animal Care and Use, and all efforts were made to minimize animal suffering and reduce the number of animals used for the experiments. For *in vitro* detection, after the rabbits were anaesthetized using isoflurane, 10^7 *T. pallidum* were first seeded on the back of the rabbit to build a standard treponemal model by forming lesions, and **Per*qdOH*** was injected into the lesions; then the images were taken under an excitation of 680 nm and an emission of 750 nm, respectively.

3. Results

3.1 Rational design, synthesis and characterization

The synthesis route and oxidation mechanism of **Per*qdOH*** are provided in Scheme 1. With the oxidation of $O_2^{\bullet-}$, the pyrocatechol groups of **Per*qdOH*** changed to carbonyl groups, which led to the transform of the fluorescence behaviour. Their structures were confirmed by ^{1}HNMR and HR-MS. We first determined the mechanism using ^{1}HNMR (Fig. S1 and S2, ESI†), and variations

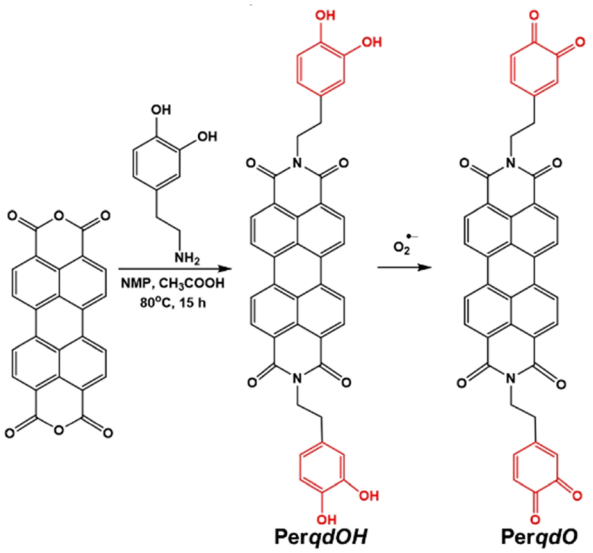

Scheme 1 The synthesis route of **P–OH** and its interaction with $O_2^{\bullet-}$.

of chemical shift between 6.0 and 9.0 ppm were in accordance with the oxidation mechanism, which clearly notified that pyrocatechol had been transformed to benzoquinone. Furthermore, the results of ^{13}CNMR (Fig. S3, ESI†) and MS (Fig. S4 and S5, ESI†) verified the conversion again.

In order to confirm the recognition toward $O_2^{\bullet-}$, UV-Vis and fluorescence measurements had been carried out. As shown in Fig. 1A, upon the addition of $O_2^{\bullet-}$, the absorption band at 490 nm decreased notably and a new absorbance band centred at 700 nm, while the absorbance band at 490 nm partly resumed after the introduction of GSH. Hence, due to the maximal absorption at 490 nm and 700 nm, they were selected as the excitation wavelengths for further study. As shown in Fig. S6 (ESI†) and Fig. 1B, with the addition of $O_2^{\bullet-}$, the fluorescence intensity of **Perq*dOH*** at 540 nm (Ex = 490 nm) decreased, and the intensity at 750 nm (Ex = 700 nm) increased meanwhile. Besides, the introduction of GSH caused the resumed fluorescence intensity at 540 nm and diminution at 750 nm. Additionally, only **Perq*dO*** exhibited obvious fluorescence under the excitation of 700 nm and emission of 750 nm (Fig. S7, ESI†). These results suggested that probe **Per*qdOH*** exhibited tuneable fluorescence due to the conversion between pyrocatechol (**Per*qdOH***) and benzoquinone (**Per*qdO***).

Subsequently, we studied the UV-vis and fluorescence of **Per*qdOH*** in the presence of various doses of $O_2^{\bullet-}$ or GSH. With the addition of $O_2^{\bullet-}$ (0–400 μM), the maximal absorption at 490 nm decreased and that at 700 nm increased in a dose-dependent manner (Fig. 2A), and a progressively enhanced and diminished fluorescence emission appeared at 750 nm (Fig. 2B) and 540 nm (Fig. S8, ESI†), separately. The concentration-dependent fluorescence response of probe *versus* $O_2^{\bullet-}$ was further investigated, and the fluorescence intensity at 750 nm revealed a linear proportion (R^2 = 0.9902) with the concentration of $O_2^{\bullet-}$ ranging from 0 to 400 μM (Fig. S9, ESI†).

What's more, as the reducing agent GSH (0–800 μM) was added to **Perq*dO***, the maximal absorption band at 490 nm recovered and the absorption band at 700 nm reduced notably (Fig. 2C), following an enhanced emission peak at 540 nm and decreased fluorescence intensity at 750 nm (Fig. 2D and Fig. S10, ESI†). The results clearly showed that our designed probe displayed satisfactory tunable response character toward oxidation and reduction.

Owing to the high reduction activity of dopamine, it has great potential to react with many oxidants, so we evaluated the selectivity of our probe **Per*qdOH*** towards different ROS

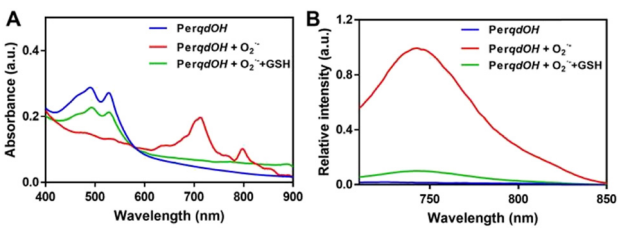

Fig. 1 (A) UV-vis spectra and (B) fluorescence spectra change after adding $O_2^{\bullet-}$ and GSH.

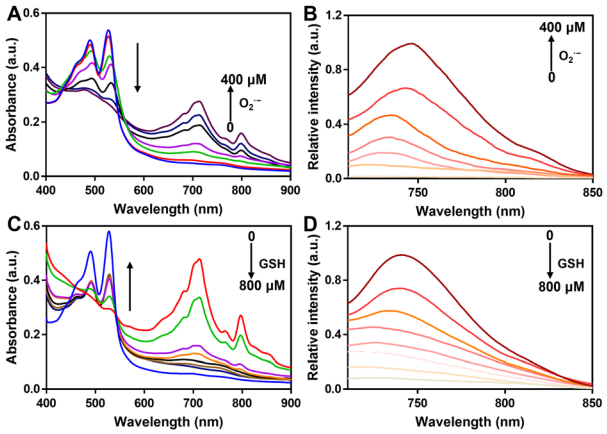

Fig. 2 Optical change of the probe under oxidation and reduction. (A) UV-Vis spectra change and (B) fluorescence change of **Per*qdOH*** after adding $O_2^{\bullet-}$ in a dose-dependent manner. (C) Uv-Vis spectra change and (D) fluorescence change of **Per*qdO*** after adding GSH in a dose-dependent manner.

including H_2O_2, $O_2^{\bullet-}$, $^1O_2$, and ClO^-. Stock solutions of HOCl and H_2O_2 were prepared by directly diluting the commercial compounds with ultra-pure water; $^{\bullet}OH$ was prepared by Fenton reaction between ferrous sulfate solution and hydrogen peroxide; $O_2^{\bullet-}$ was delivered by dissolving potassium superoxide in DMSO; and $^1O_2$ was obtained by irradiating Rose Bengal with laser (660 nm, 20 mW). As shown in Fig. S11A (ESI†), only the addition of $O_2^{\bullet-}$ induced the increased absorption band at 700 nm, the decreased fluorescence intensity at 540 nm (Fig. S11B, ESI†) and the appearance of maximal fluorescence enhancement at 750 nm (Fig. S11C, ESI†), whereas the variations with the other analytes were negligible. Additionally, the fluorescence image, which was taken under an excitation of 680 nm and an emission of 750 nm, clearly demonstrated the high specificity of **Per*qdOH*** towards $O_2^{\bullet-}$ according to the apparent fluorescence after treatment with $O_2^{\bullet-}$ (Fig. S11D, ESI†).

3.2 Monitoring and imaging of $O_2^{\bullet-}$ *in vitro*

Before carrying out the cell imaging studies of **Per*qdOH***, cytotoxicity assays revealed that **Per*qdOH*** within 40 μM is suitable for bioimaging application (Fig. S12, ESI†). Next, we monitored the transport of probe **Per*qdOH*** in cells after staining the mitochondria (MitoTracker red) and nucleus (Hoechst 33342), and this directly showed that probe **Per*qdOH*** had crossed the cell membrane and gradually accumulated in the cells after incubation for 30 min, and then filled the cytoplasm at 60 min, which could be chosen as the time point of detection internalization time (Fig. 3). Furthermore, probe **Per*qdOH*** was co-located with mitochondria, implying that the changes of $O_2^{\bullet-}$ in the mitochondria can be monitored.

In order to demonstrate the capability for imaging endogenous $O_2^{\bullet-}$ in living cells, we used several groups of cell lines for test. After 1 hour pre-incubation with **Per*qdOH***, $O_2^{\bullet-}$ was first added into the cells, and laser confocal microscopy was employed for imaging. As shown in Fig. S13 (ESI†), compared to the probe **Per*qdOH*** alone in the cells, green fluorescence

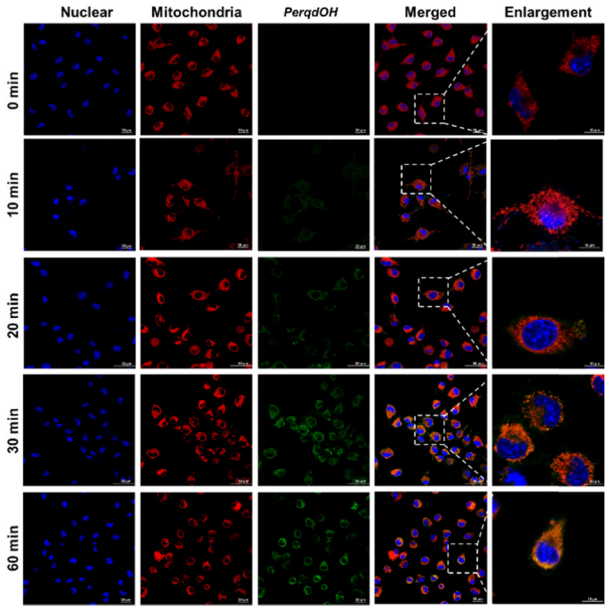

Fig. 3 Intracellular trafficking of 40 μM Per*qdOH* in cells at different periods of time (0–60 min). Mito tracker (red) and Hoechst 33342 were used to stain mitochondria and nucleus, separately.

(**Per*qdOH***) was rarely noticeable in the group treated with $O_2^{\bullet-}$, while red fluorescence (**Per*qdO***) was progressively enhanced. Then we employed the probe for endogenous $O_2^{\bullet-}$ detection. For this purpose, B16 cells and RAW 264.7 cells were treated with phorbol-12-myristate-13-acetate (PMA) after co-incubating with probe Per*qdOH* for 1 h.

PMA is considered as an endogenous $O_2^{\bullet-}$ trigger, which would induce endogenous $O_2^{\bullet-}$ after incubation with cells.[37,38] The increase in red fluorescent channel and decrease in green fluorescent channel were observed in a time-dependent and dose-dependent manner in PMA-treated B16 cells (Fig. 4). Besides, both fluorescence intensity in the green channel and the red channel stayed steady as the culture time elapsed continually, suggesting that the amount of produced and consumed endogenous $O_2^{\bullet-}$ was balanced after 24 hour incubation with PMA. PMA-treated RAW 264.7 cells also displayed similar fluorescence behaviour to B16 cells (Fig. S14, ESI†).

Additionally, we determined the reversible capability of probe **Per*qdOH*** in cell lines by employing GSH as the reductant after treatment with PMA. As displayed in Fig. S15 (ESI†), the fluorescence intensity in the green channel recovered with the addition of GSH, while the red fluorescence became weaker meanwhile, illustrating that the probe could reflect the oxidative conditions *via* the reversible fluorescence behaviour. In a word, our designed **Per*qdOH*** has potential for the detection of endogenously generated $O_2^{\bullet-}$ in cellular systems under different conditions.

3.3 Monitoring and imaging of oxidative conditions caused by *T. pallidum*

As reported previously, *T. pallidum* is eliminated by immune cells at the early stage of infection.[39] Thus, we focus on the

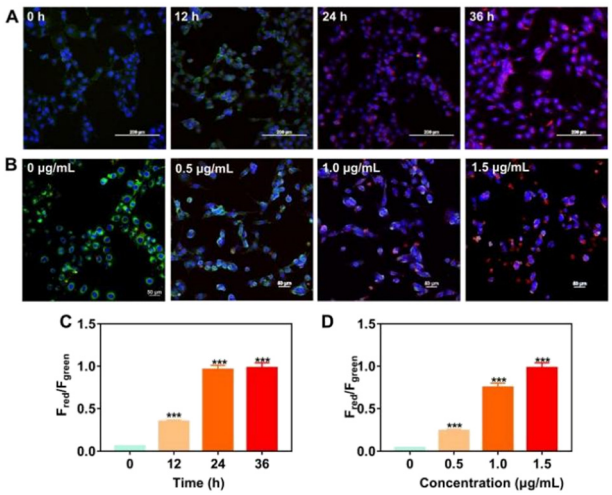

Fig. 4 Monitoring endogenous $O_2^{\bullet-}$ in cells. Fluorescence images of B16 cells after co-incubation with PMA in (A) a time-dependent manner (from 0 h to 36 h) and (B) a dose-dependent manner (0-1.5 μg mL^{-1}). (C) and (D) The quantitative analysis of the relative fluorescence intensity.

production of intracellular $O_2^{\bullet-}$ during the clearance. It was first found that the exposure of synthesized **Per*qdOH*** was nearly nontoxic for *T. pallidum* (Fig. S16, ESI†). We then monitored the interaction between macrophages and *T. pallidum in vitro* using the probe. According to Fig. 5, we found the increased red fluorescence intensity as the MOI of treated *T. pallidum* changed from $1:10^1$ to $1:10^3$ after 24 hour incubation, which indicated that the endogenous $O_2^{\bullet-}$ had been produced during co-culture between *T. pallidum* and RAW 264.7 cells.

Since probe **Per*qdOH*** could detect exogenous and endogenous $O_2^{\bullet-}$, we envisaged that the probe could have the potential to detect $O_2^{\bullet-}$ under *in vivo* conditions. Therefore, New Zealand white rabbits were utilized as the primary syphilis model. After *T. pallidum*-induced lesions on the back appeared, probe **Per*qdOH*** was injected into the lesions and the adjacent skin. Obviously, as shown in Fig. 6A and B, the signal of **Per*qdO***

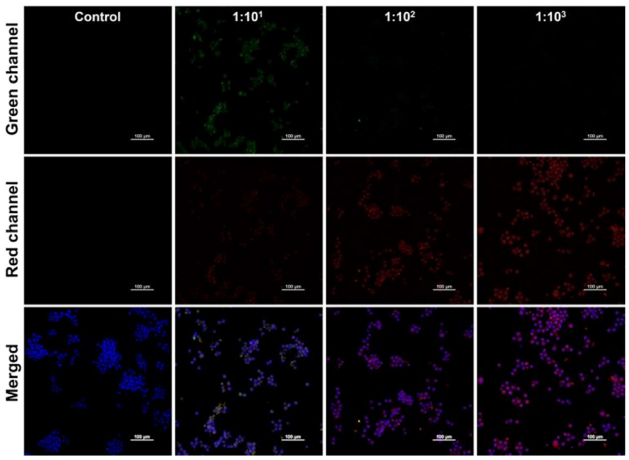

Fig. 5 Fluorescence images of simulating infection by different MOIs ($1:10^1$, $1:10^2$, $1:10^3$) of *T. pallidum in vitro*. Scale bar: 100 μm.

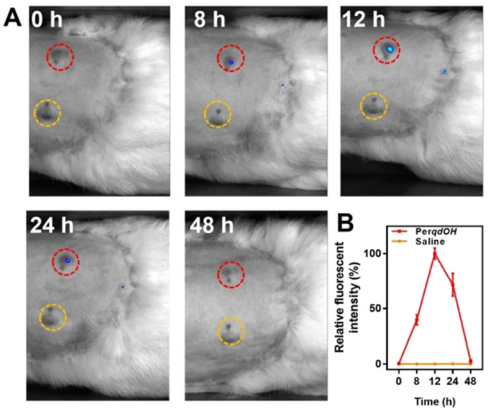

Fig. 6 *In vivo* monitoring of endogenous $O_2^{\bullet-}$ in the lesions of a primary syphilis model. (A) The images of fluorescence change in the lesions at different periods of time. (B) The relative statistics. The red circle marks the lesion injected with **Per*qdOH***, and the orange circle marks the lesion injected with saline, while the green circle marks the adjacent area injected with **Per*qdOH***.

(Ex = 680 nm, Ex = 750 nm) in the lesions raised 8 hours after injection, and the intensity became maximal after another 4 hours, followed by a decreased signal of the probe due to the clearance by the immune system in the subsequent period. In a word, probe **Per*qdOH*** is an efficient probe for monitoring $O_2^{\bullet-}$ during *T. pallidum* infection under *in vivo* conditions.

4. Discussion

Syphilis can be regard as an inflammatory disease due to the tissue destruction character of *T. pallidum* through the whole process, and this process is closely related to ROS. Monitoring ROS is critical to determine the inflammatory process caused by the pathogen. $O_2^{\bullet-}$ is one of the primary ROS, which could cause great damage to the cells during inflammation by causing oxidative stress. Numerous probes have been designed to detect ROS, but many of them failed to be further used owing to the lack of stability under irradiation. We thus designed a fluorescence tuneable probe (**Per*qdOH***) which could exhibit a fluorescence shift under the stimulation of $O_2^{\bullet-}$.

We first determined the fluorescence behaviour change of the designed probe **Per*qdOH*** using UV-Vis spectrum and fluorescence spectrum. The results suggested that the maximal absorption band of **Per*qdOH*** would shift from 490 nm to 700 nm with the addition of $O_2^{\bullet-}$, following the decrease in the emission intensity at 540 nm (Ex = 490 nm) and a progressive increase in the fluorescence intensity at 750 nm (Ex = 700 nm) meanwhile, due to the conversion from pyrocatechol to benzoquinone according to ^{1}HNMR and MS and ^{13}CNMR. Besides, the introduction of reductant GSH led to the recovered fluorescence intensity at 540 nm. Also, the probe displayed unique selectivity towards $O_2^{\bullet-}$. Next, *in vitro* fluorescence behaviour was used to investigate the detection of intracellular $O_2^{\bullet-}$. With the addition of $O_2^{\bullet-}$ into the cells, the fluorescence intensity in the green channel decreased and the intensity in the red channel increased, suggesting that probe **Per*qdOH*** in the cells has been oxidized to **Per*qdO*** by $O_2^{\bullet-}$. Furthermore, PMA was used to trigger endogenous $O_2^{\bullet-}$, and our designed **Per*qdOH*** responsively exhibited obvious fluorescence transform capability during the excitation of PMA, displaying the potential to monitor intracellular $O_2^{\bullet-}$. As macrophage is the first-stage of defence against *T. pallidum*, we simulated the immunity process of syphilis by infecting RAW 264.7 cells with *T. pallidum*, and monitored the intracellular $O_2^{\bullet-}$ using the probe. We noticed decreasing green fluorescence intensity and increasing red fluorescence intensity with increasing number of pathogens, suggesting that *T. pallidum* could induce the generation of $O_2^{\bullet-}$ during phagocytosis. Additionally, *in vivo* detection in the lesions of the primary syphilis model proved to be an efficient tool for monitoring treponemal-related $O_2^{\bullet-}$ response in living systems.

5. Conclusions

In conclusion, we have rationally designed a fluorescence tuneable probe **Per*qdOH*** to enable the monitoring of intracellular $O_2^{\bullet-}$. The emission of the synthesized probe could shift from 540 nm to 750 nm with the addition of $O_2^{\bullet-}$ because the pyrocatechol (**Per*qdOH***) had been oxidized to benzoquinone (**Per*qdO***), while the fluorescence at 540 nm recovered under the reduction of GSH, representing that fluorescence is tuneable under oxidation and reduction conditions. Besides, probe **Per*qdOH*** could responsively detect exogenous and endogenous $O_2^{\bullet-}$ in cells, especially during the infection of *T. pallidum* in the host cells *in vivo* and *in vitro*. Taken together, our synthesized probe **Per*qdOH*** might prove to be an efficient tool for monitoring the process of inflammatory *T. pallidum* infection in living systems.

Author contributions

JDZ and WQL designed and performed the experiment. JLH, SG and WQL were responsible for data collation. WQL and JLH drafted the manuscript. SG, GFL, and JDZ edited and revised the manuscript draft. JDZ, GFL and YHL were responsible for providing funds and unified management of work. All authors read and approved the final manuscript.

Conflicts of interest

There are no conflicts to declare.

Acknowledgements

This research was supported by the National Key Research and Development Program (2021YFC2302200), the Natural Science Fund of Guangdong Province for Distinguished Young Scholars (2022B1515020089), the National Natural Science Foundation of China (82272248, 81972019, 82102444), Training project of National Science Foundation for Outstanding/Excellent Young

Scholars of Southern Medical University (C620PF0217, 2019RC01), and Zhongnanshan Medical Foundation of Guangdong Province (ZNSA-2021012; Guang Dong Province, China).

References

1 R. W. Peeling, D. Mabey, M. L. Kamb, X. S. Chen, J. D. Radolf and A. S. Benzaken, *Nat. Rev. Dis. Primers*, 2017, **3**, 17073.
2 J. B. Taxy and T. Cibull, *Am. J. Surg. Pathol*, 2020, **44**, 1274–1281.
3 Z. Li, J. Zhang, Y. Huang, J. Zhai, G. Liao, Z. Wang and C. Ning, *Coord. Chem. Rev.*, 2022, **471**, 214723.
4 S. Tuddenham, M. M. Hamill and K. G. Ghanem, *JAMA*, 2022, **327**, 161–172.
5 L. R. Lin, W. Liu, X. Z. Zhu, Y. Y. Chen, Z. X. Gao, K. Gao, M. L. Tong, H. L. Zhang, Y. Xiao, W. D. Li, S. L. Li, H. L. Lin, L. L. Liu, Z. X. Fang, J. J. Niu, Y. Lin and T. C. Yang, *BMC Immunol.*, 2018, **19**, 28.
6 A. Flamm, K. Parikh, Q. Xie, E. J. Kwon and D. M. Elston, *J. Am. Acad. Dermatol.*, 2015, **73**, 1025–1030.
7 A. Flamm, V. M. Alcocer, V. Kazlouskaya, E. J. Kwon and D. Elston, *J. Am. Acad. Dermatol.*, 2020, **82**, 156–160.
8 A. R. Cruz, L. G. Ramirez, A. V. Zuluaga, A. Pillay, C. Abreu, C. A. Valencia, C. La Vake, J. L. Cervantes, S. Dunham-Ems, R. Cartun, D. Mavilio, J. D. Radolf and J. C. Salazar, *PLoS Neglected Trop. Dis.*, 2012, **6**, e1717.
9 J. E. Bennett, R. Dolin and M. J. Blaser, *Mandell, douglas, and bennett's principles and practice of infectious diseases E-book*, Elsevier Health Sciences, 2019.
10 S. Liu, S. Wang, Y. Wu, F. Zhao, T. Zeng, Y. Zhang, Q. Zhang and D. Gao, *Sci. China: Life Sci.*, 2010, **53**, 229–233.
11 H. J. Forman and M. Torres, *Am. J. Respir. Crit. Care Med.*, 2002, **166**, S4–S8.
12 G. Liao, F. He, Q. Li, L. Zhong, R. Zhao, H. Che, H. Gao and B. Fang, *Prog. Mater. Sci.*, 2020, **112**, 100666.
13 G. Liao, L. Zhang, C. Li, S.-Y. Liu, B. Fang and H. Yang, *Matter*, 2022, **5**, 3341–3374.
14 Z. Mo, X. Pan, X. Pan, L. Ye, H. Hu, Q. Xu, X. Hu, Z. Xu, J. Xiong, G. Liao and S. Yang, *J. Mater. Chem. B*, 2022, **10**, 8760–8770.
15 Z. Qin, M. Qiu, Q. Zhang, S. Yang, G. Liao, Z. Xiong and Z. Xu, *J. Mater. Chem. B*, 2021, **9**, 8882–8896.
16 L. Zhang, G. Oudeng, F. Wen and G. J. B. R. Liao, *Biomater. Res.*, 2022, **26**, 61.
17 H. Wang, K. Wan and X. Shi, *Adv. Mater.*, 2019, **31**, e1805368.
18 Z. Li, T. Liang, S. Lv, Q. Zhuang and Z. Liu, *J. Am. Chem. Soc.*, 2015, **137**, 11179–11185.
19 J. Zheng, Y. Wu, D. Xing and T. Zhang, *Nano Res.*, 2019, **12**, 931–938.
20 K. Kobayashi, *Chem. Rev.*, 2019, **119**, 4413–4462.
21 J. Fang, T. Seki and H. Maeda, *Adv. Drug Delivery Rev.*, 2009, **61**, 290–302.
22 R. Liu, L. Zhang, Y. Chen, Z. Huang, Y. Huang and S. Zhao, *Anal. Chem.*, 2018, **90**, 4452–4460.
23 W. Lin, H. Liu, L. Chen, J. Chen, D. Zhang, Q. Cheng, F. Yang, Q. Zeng and T. Chen, *Nano Today*, 2021, **38**, 101124.
24 A. Singh, R. Kukreti, L. Saso and S. Kukreti, *Molecules*, 2019, **24**, 1583.
25 I. S. Harris and G. M. DeNicola, *Trends Cell Biol.*, 2020, **30**, 440–451.
26 C. Zhou, X. Zhang, W. Zhang, J. Duan and F. Zhao, *J. Clin. Lab. Anal.*, 2019, **33**, e22890.
27 L. R. Lin, Y. Xiao, W. Liu, Y. Y. Chen, X. Z. Zhu, Z. X. Gao, K. Gao, M. L. Tong, H. L. Zhang, S. L. Li, H. L. Lin, W. D. Li, X. M. Liang, Y. Lin, L. L. Liu and T. C. Yang, *BMC Infect. Dis.*, 2018, **18**, 101.
28 H. Sies and D. P. Jones, *Nat. Rev. Mol. Cell Biol.*, 2020, **21**, 363–383.
29 B. Kong, T. Yang, F. Cheng, Y. Qian, C. Li, L. Zhan, Y. Li, H. Zou and C. Huang, *J. Colloid Interface Sci.*, 2022, **611**, 545–553.
30 X. Liu, Z. Yan, Y. Sun, J. Ren and X. Qu, *Chem. Commun.*, 2017, **53**, 6215–6218.
31 B. Yang, Y. Chen and J. Shi, *Chem. Rev.*, 2019, **119**, 4881–4985.
32 Y. Wei, Y. Liu, Y. He and Y. Wang, *J. Mater. Chem. B*, 2021, **9**, 908–920.
33 P. Xu and G. Liao, *Materials*, 2018, **11**, 1616.
34 J. Zheng, Q. Zeng, R. Zhang, D. Xing and T. Zhang, *J. Am. Chem. Soc.*, 2019, **141**, 19226–19230.
35 W. Zhang, P. Li, F. Yang, X. Hu, C. Sun, W. Zhang, D. Chen and B. Tang, *J. Am. Chem. Soc.*, 2013, **135**, 14956–14959.
36 P. Gao, W. Pan, N. Li and B. Tang, *Chem. Sci.*, 2019, **10**, 6035–6071.
37 Y. Wang, K. M. Dillon, Z. Li, E. W. Winckler and J. B. Matson, *Angew. Chem., Int. Ed.*, 2020, **59**, 16698–16704.
38 Y. Zhao and M. D. Pluth, *Angew. Chem., Int. Ed.*, 2016, **55**, 14638–14642.
39 S. L. Xu, Y. Lin, X. Z. Zhu, D. Liu, M. L. Tong, L. L. Liu, T. C. Yang and L. R. Lin, *J. Eur. Acad. Dermatol. Venereol.*, 2020, **34**, 2111–2119.

